



## Analysis of the digital null-seeker architecture's steady-state error for GNSS receivers

Alban Rakipi <sup>\*1</sup>, Olimpjon Shurdi <sup>1</sup>, Aleksander Biberaj <sup>1</sup>

<sup>1</sup>Polytechnic University of Tirana, Department of Electronics and Telecommunications, Albania,  
[arakipi@fti.edu.al](mailto:arakipi@fti.edu.al), [oshurdi@fti.edu.al](mailto:oshurdi@fti.edu.al), [abiberaj@fti.edu.al](mailto:abiberaj@fti.edu.al)

Cite this study: Rakipi, A., Shurdi, O., & Biberaj, A. (2023). Analysis of the digital null-seeker architecture's steady-state error for GNSS receivers. *Engineering Applications*, 2 (2), 126-135

### Keywords

Null-seeker  
 GNSS  
 Tracking  
 Noise bandwidth  
 Receiver

### Research Article

Received:08.03.2023  
 Revised: 03.05.2023  
 Accepted: 17.05.2023  
 Published:26.05.2023



### Abstract

In this paper, the architecture of closed-loop synchronizers is studied. For a GNSS (Global Navigation Satellite System) receiver, the fine estimation of the code delay and Doppler frequency is generally performed by two concatenated null-seekers, the PLL (Phase Lock Loop), and the DLL (Delay Lock Loop). The null-seeker is implemented, tested and analyzed in a software receiver. The noise equivalent bandwidth, integration time and different incoming signal structures are considered for testing and performance evaluation. Different tests have been performed by changing the input signal from a step unit function to a ramp signal and finally to a parabolic shaped signal. The noise-free steady state value of estimation error is evaluated. The type of loop filter defines the tracking capability of the loop. The estimation error must quickly reach zero for a certain input model and any initial error, in the absence of noise.

## 1. Introduction

Four separate worldwide GNSS systems are now available, with Galileo and BeiDou attaining full operating capacity [1]. Synchronizing with the visible satellite signals is an important function of any GNSS receiver [2]. To detect and track the GNSS signals, the receiver employs the auto-correlation principle. It generates a transmitted GNSS signal copy of a single satellite inside the receiver and correlates this replica signal with the received signal [3]. The receiver must first produce a local signal that matches the incoming signal from the satellite before it can give measurements to compute a position, velocity, and timing (PVT) solution. This is done in two stages, namely acquisition and tracking [4]. The objective of the acquisition stage is to find coarse estimates of the Doppler shift and timing offset [5]. An extremely crucial component is the carrier tracking loop, which is utilized to synchronize the local carrier with the incoming signals. Commonly used in the carrier tracking loop, the phase lock loop (PLL) is incredibly fragile, especially in difficult environments [4].

The tracking bandwidth and integration time play an important role on accuracy and dynamic stress tolerance. To reduce the noise and improve accuracy, the tracking bandwidth should be narrow and the integration time long [5]. As a result of the oscillator noise and dynamics on the carrier tracking loop, the bandwidth cannot be reduced arbitrarily. Otherwise, it will cause the phenomena of lock-lose [6]. Due to the complicated environment in the tracking system, accurate models and noise statistics are difficult to be known [4]. For a high sensitivity receiver, no matter whether in acquisition or tracking, the key problem is to extend the coherent time [6]. In [7] the focus is on the process of carrier phase tracking in a scalar PLL. The authors in [8] propose an accurate receiver clock drift estimation method to increase prediction effective time.

In this work is implemented, tested and analyzed a digital synchronization loop architecture in a software receiver. The noise equivalent bandwidth, integration time and different incoming signal structures are considered for testing and performance evaluation.

## 2. Material and Method

In a conventional GNSS receiver, the acquisition and tracking of the signals are all processed by the hardware. However, in a software GNSS receiver, the signal is digitized using an analog-to-digital converter (ADC). Acquisition and tracking of GNSS satellites are the key processes involved in a GNSS receiver. Software GNSS receivers capture the RF modulated signals at L1/E1 frequency, down convert them to an intermediate frequency (IF), digitize them, and perform signal processing to extract the position information from the navigation message. The digitized input signal is then processed using the software receiver [9] depicted in Figure 1.

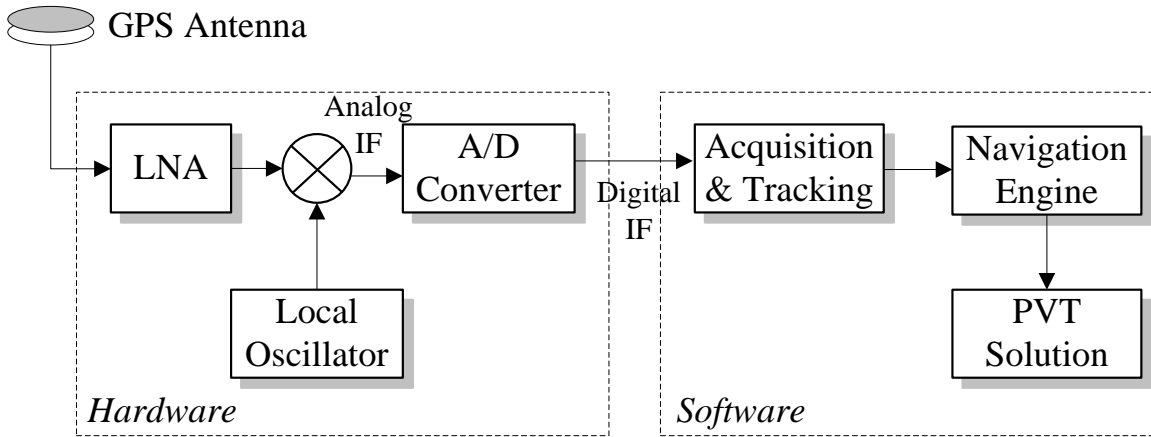


Figure 1. Simplified structure of a GNSS receiver

The architecture of a closed-loop synchronizer, namely the null-seeker is given in Figure 2 [3]. The input signal  $y[k, \xi]$  is combined with a locally generated reference signal  $x_{ref} = (k, \hat{\xi}[k])$  which has typically the same basic structure as the input signal, apart from the presence of noise and other nuisances. It is characterized by the estimated parameter computed during the previous iteration  $\hat{\xi}[k]$ . The discrimination function can transform  $z[k, \xi]$  into a different metric (error signal).  $e_{\xi}[k, \xi]$  value depends on and is proportional to the estimation error  $e_{\xi}[k, \xi] \propto \xi - \hat{\xi}[k]$ . A fundamental property is that one of its zeros corresponds to the searched value of the parameter to be estimated.

The key operation of a null seeker is to find a zero of its discrimination function (iteratively). The discrimination function  $S(\cdot)$  in (1) can be nonlinear, but it is convenient to study the overall system in its linearity region therefore:  $e_{\xi}[k, \xi] \approx \beta \cdot (\xi - \hat{\xi}[k])$  where  $\beta$  is the slope of the S-curve in  $\xi - \hat{\xi}[k] = 0$ .

$$e_{\xi}[k, \xi] = S(\xi - \hat{\xi}[k]) \quad (1)$$

The Low-pass loop filter smoothens the error signal to reduce the contribution of the noise  $w[k]$  and it still preserves the reactivity of the loop to the dynamics of the parameter to be estimated. The new estimated parameter is extracted from the filtered error signal.

$$\hat{\xi}[k + 1] = \hat{\xi}[k] + e_{\xi}[k] \quad (2)$$

The updating rule in (2) followed by the "Delay" block, represents an IIR digital filter, with input  $e_{\xi}[k]$  and output  $\hat{\xi}[k]$ .

Z-transform is given by Equation 3:

$$e(z) = \sum_{k=-\infty}^{+\infty} e[k]z^{-k} \quad (3)$$

and update rule transfer function is  $z\hat{\xi}(z) = \hat{\xi}(z) + e_{\xi}(z)$ .

Transfer function from  $e_{\xi}(k)$  to  $\hat{\xi}(k)$  can be written in the form of Equation 4:

$$D(z) = \frac{\hat{\xi}(z)}{e_{\xi}(z)} = \frac{1}{z-1} = \frac{z^{-1}}{1-z^{-1}} \quad (4)$$

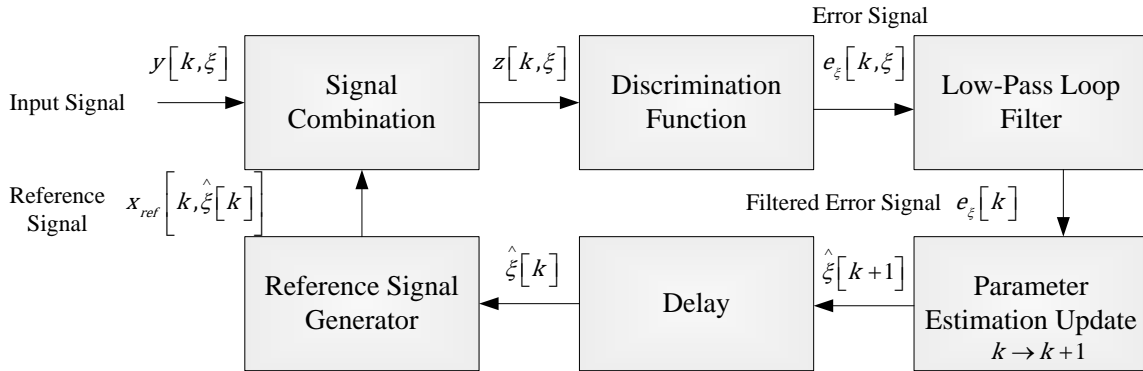


Figure 2. Null-seeker architecture

As the received signal is noisy, then the error signal contains an additive noise component  $e_{\xi}[k, \xi] = \beta\delta_{\xi}[k] + \eta[k]$  where  $\delta_{\xi}[k] = \xi - \hat{\xi}[k]$  is the instantaneous error and  $\eta[k]$  is a discrete-time random process, white and Gaussian. It is independent from  $\delta_{\xi}[k]$  and “circulates” within the loop coupled with  $\delta_{\xi}[k]$ . Since the variables inside the loop are updated step by step, the theory of discrete-time signals is the most adequate to study the loop operations.

The null-seeker architecture can be reduced to the equivalent linear system depicted in Figure 3 where only the parameter to be estimated appears. From the point of view of the system performance,  $\delta_{\xi}[k]$  represents the instantaneous estimation error, which we would like to be exactly equal to zero. The estimation error  $\delta_{\xi}[k]$  is the sum of two contributes:  $\xi[k]$  and  $\eta[k]$ . We would like the first component to be zero and the second component (jitter) be as small as possible, at least after an initial transient (as small as possible).

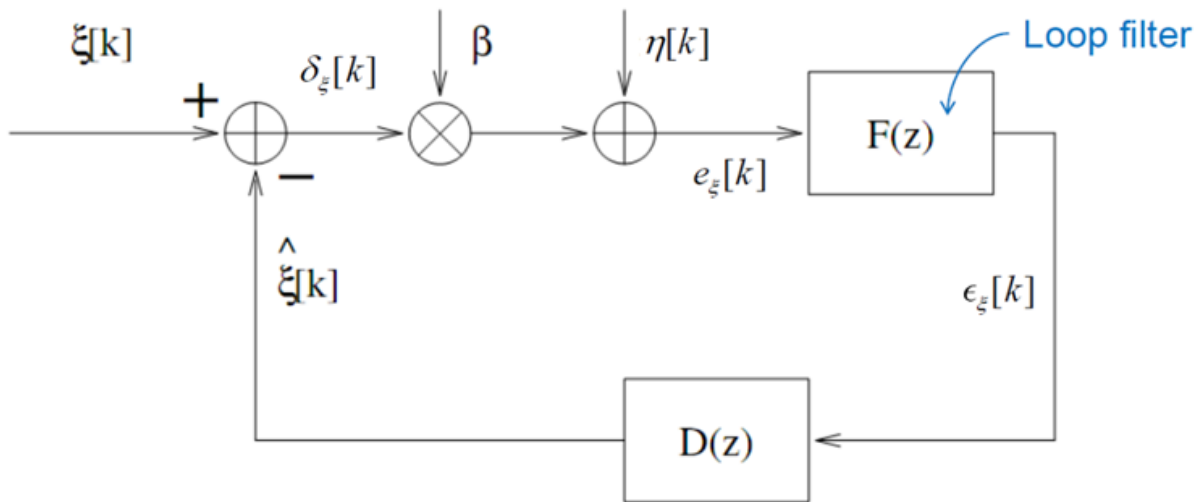


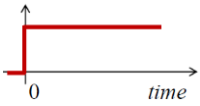
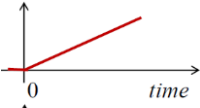
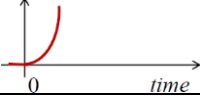
Figure 3. Equivalent linear system of the null-seeker architecture

### 3. Simulation and Results

To test the behavior of the null-seeker, the block diagram in Figure 1, is implemented at the software level using MATLAB. Different tests have been performed by changing the input signal from a unit step function to a ramp signal and finally to a parabolic shaped signal. The other two variable parameters of the simulations are respectively the order of the filter and the product of the equivalent noise bandwidth with the integration time. The steady-state estimation error is evaluated and plotted in for all the tests.

The input signals considered are shown in Table 1. The step input parameter can be considered a constant unknown random variable. The ramp input represents a system that transmits a pure carrier, while it moves at constant speed  $v$ . The parabolic function represents a system that transmits a pure carrier while moving at a constant acceleration  $a$ .

**Table 1.** Three input signal models

Input	Graph	Mathematical expression
Step		$\xi_1[k] = Au[k] = \begin{cases} 0 & k < 0 \\ A & k \geq 0 \end{cases}$
Ramp		$\xi_2[k] = Ak u[k] = \begin{cases} 0 & k < 0 \\ Ak & k \geq 0 \end{cases}$
Parabolic		$\xi_3[k] = Ak^2 u[k] = \begin{cases} 0 & k < 0 \\ Ak^2 & k \geq 0 \end{cases}$

The Z-transform of the three input models, and corresponding estimation error in the Z-domain are shown in Table 2.

**Table 2.** Three input signal models

Input	Z-transform	Estimation error in Z-domain
Step	$\xi_1(z) = A \frac{z}{z-1}$	$\delta_{\xi,1}(z) = \frac{Az}{(z-1) + \beta F(z)}$
Ramp	$\xi_2(z) = A \frac{z}{(z-1)^2}$	$\delta_{\xi,2}(z) = \frac{1}{(z-1) + \beta F(z)} \frac{Az}{(z-1)}$
Parabolic	$\xi_3(z) = A \frac{z(z+1)}{(z-1)^3}$	$\delta_{\xi,3}(z) = \frac{1}{(z-1) + \beta F(z)} \frac{Az(z+1)}{(z-1)^2}$

### 3.1. First order loop with unit step input

One can observe from Figure 4 to Figure 5 that an increase of one order of magnitude of the loop noise equivalent bandwidth (from  $B_{eqT_s} = 0.0005$  to  $B_{eqT_s} = 0.005$ ) decreases  $k$ , and the estimation error decreases with the same order of magnitude. So, the integration time is decreased by an order of magnitude. Another important remark that can be derived is that in order to minimize the steady-state error, the noise equivalent bandwidth should be increased.

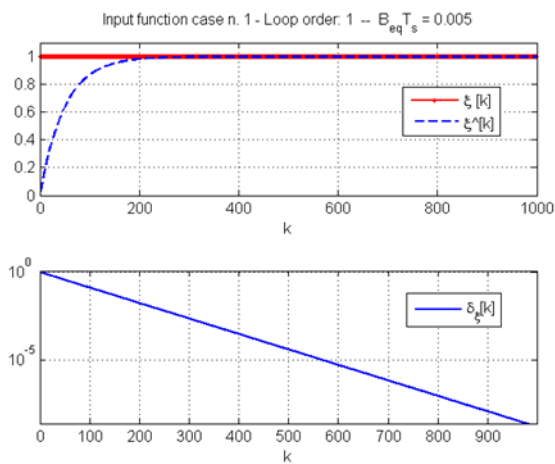


**Figure 4.** Plot of the estimation error  $\delta_{\xi}[k]$  in the logarithmic scale, for step input

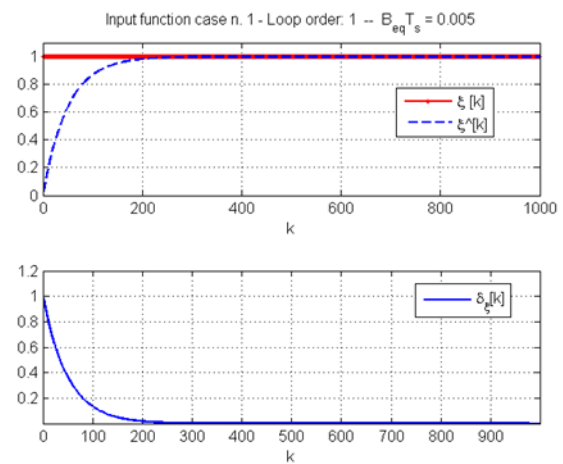


**Figure 5.** Plot of the steady state error  $\delta_{\xi}[k]$  for a step input and  $B_{eqT_s} = 0.005$

The plot in Figure 8 is for  $k=1000$  samples, which obviously are not enough to correctly measure the acquisition time and so the MATLAB script is modified using  $k = 10000$ , obtaining the plot on Figure 9. The increased number of samples allows us to correctly determine the acquisition time.

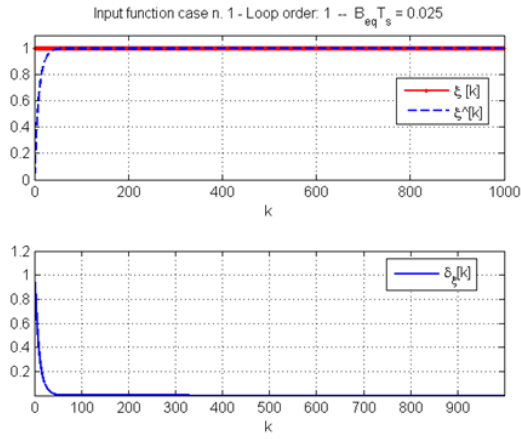


**Figure 6.** Plot of the steady state error  $\delta_{\xi}[k]$  for a step input and  $B_{eq}T_s = 0.025$

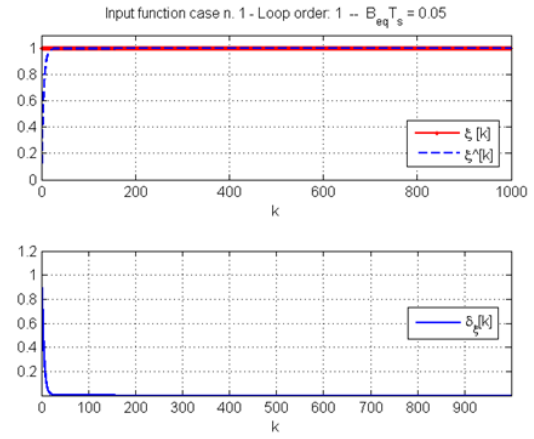


**Figure 7.** Plot of the steady state error  $\delta_{\xi}[k]$  for a step input and  $B_{eq}T_s = 0.05$

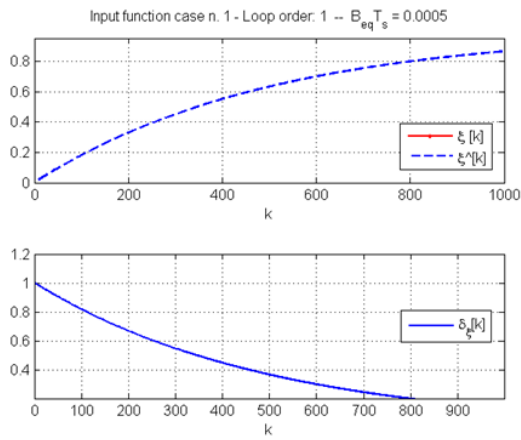


**Figure 8.** Plot of the steady state error  $\delta_{\xi}[k]$  for a step input,  $B_{eq}T_s = 0.0005$  and  $k=1000$

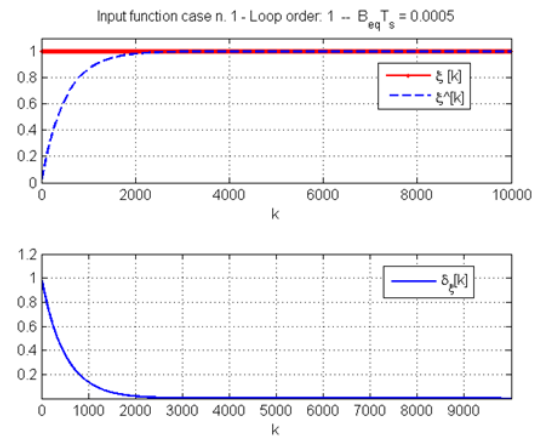


**Figure 9.** Plot of the steady state error  $\delta_{\xi}[k]$  for a step input,  $B_{eq}T_s = 0.0005$  and  $k=10000$

### 3.2. First order loop with ramp input

After plotting the estimation error  $\delta_{\xi}[k]$  for a ramp input, we observe a quadratic characteristic of the estimation error, which achieves the steady state value  $\delta_{\xi}[k] = 5$  after  $k = 456$  samples.

From the Final Value Theorem, we have this relationship for a ramp input:

$$\lim_{k \rightarrow \infty} \delta_{\xi,2}^{(I)}[k] = \lim_{z \rightarrow 1} \frac{Az}{(z-1) + \beta\gamma} = \frac{A}{\beta\gamma}$$

Substituting the values of the filter's parameters  $A$ ,  $\beta$ , and  $\gamma$  from the MATLAB script, we obtain this final value according to the Final Value Theorem:

$a_1 = 0.1$ ,  $\beta=1$  and

$$\gamma = \frac{4 \cdot B_{eq}T_s}{\beta} = \frac{4 \cdot 0.005}{1} = 0.02$$

$$\lim_{k \rightarrow \infty} \delta_{\xi,2}^{(I)}[k] = \frac{A}{\beta\gamma} = \frac{a_1}{\beta\gamma} = \frac{0.1}{1 \cdot 0.02} = 5$$

So, is obtained the same value of the steady state error from the MATLAB simulation and from the Final Value Theorem  $\delta_{\xi}[k] = 5$ .

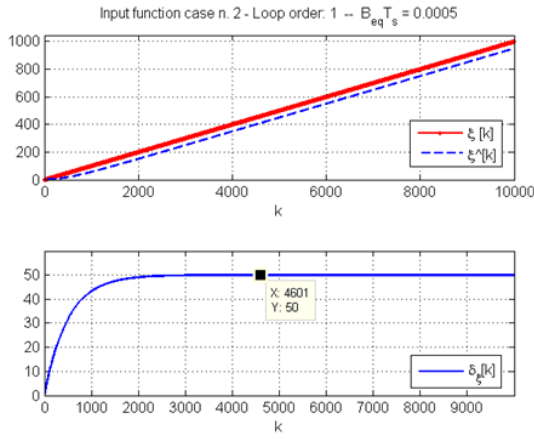


Figure 10. Plot of the steady state error  $\delta_\xi[k]$  for a ramp input,  $B_{eq}T_s = 0.0005$

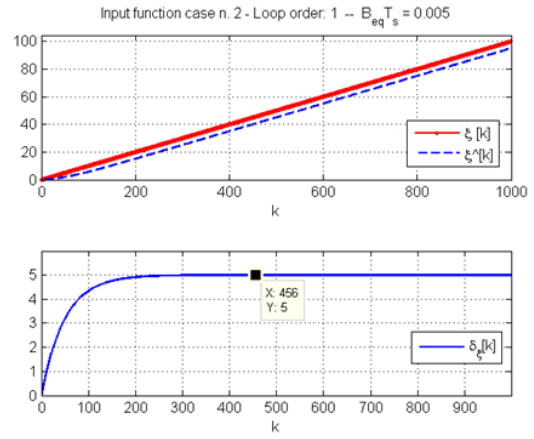


Figure 11. Plot of the steady state error  $\delta_\xi[k]$  for a ramp input,  $B_{eq}T_s = 0.005$

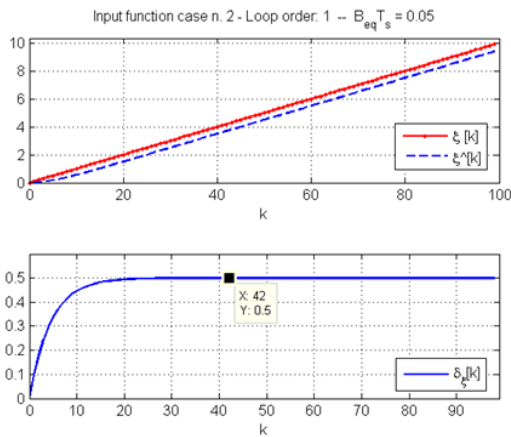


Figure 12. Plot of the steady state error  $\delta_\xi[k]$  for a ramp input,  $B_{eq}T_s = 0.05$

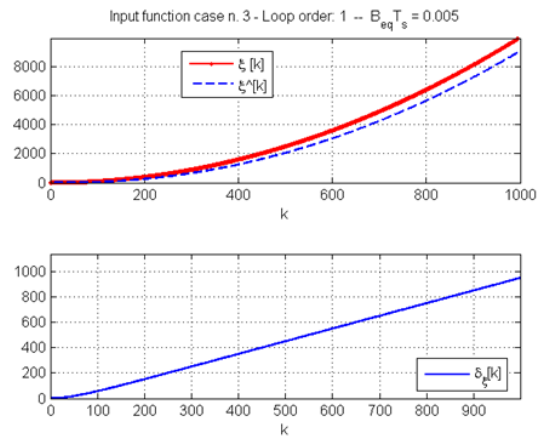


Figure 13. Plot of the steady state error  $\delta_\xi[k]$  for a parabolic input,  $B_{eq}T_s = 0.005$

In Table 3 are summarized the results for different values of the noise equivalent bandwidth product with integration time. Observing the plots and referring to the values of the estimation error  $\delta_\xi[k]$  from Table 3, in three different cases of  $B_{eq}T_s$ , we can derive the relationship between the estimation error and the loop noise equivalent bandwidth  $B_{eq}T_s$  as following:

An increase of one order of magnitude of the loop noise equivalent bandwidth (from  $B_{eq}T_s = 0.0005$  to  $B_{eq}T_s = 0.005$  and finally to  $B_{eq}T_s = 0.05$ ) decreases the estimation error with the same order of magnitude (from 50 to 5, to 0.5) and so the time is decreased by an order of magnitude (10 times after each iteration).

From this conclusion we can draw another important remark that to minimize the steady-state error, is needed to increase the noise equivalent bandwidth  $B_{eq}T_s$ .

**Table 3.** The effect of the increase of  $B_{eq}T_s$  on the steady-state error

$B_{eq}T_s$	$\delta_\xi[k]$	$k$
0.0005	50	4601
0.005	5.0	456
0.05	0.5	42

### 3.3. First order loop with parabolic input

After plotting  $\delta_\xi[k]$  as a function of the number of samples  $k$  for the parabolic input, Figure 12 is obtained in which can be easily observed that the estimation error  $\delta_\xi[k]$  is unbounded because of the unlimited characteristic of the parabolic input. To verify if it is possible to have a limited maximum value for the estimation error  $\delta_\xi[k]$  we

run the script for different values of  $B_{eq}T_s$  and the plots in Figures 13-14 were obtained. It is obvious that it is not possible to have a limited maximum value for  $\delta_\xi[k]$  because in all the cases it is an unlimited function.

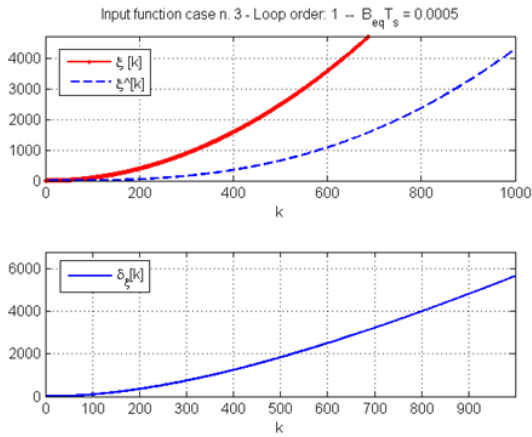


Figure 14. Plot of the steady state error  $\delta_\xi[k]$  for a parabolic input,  $B_{eq}T_s = 0.0005$

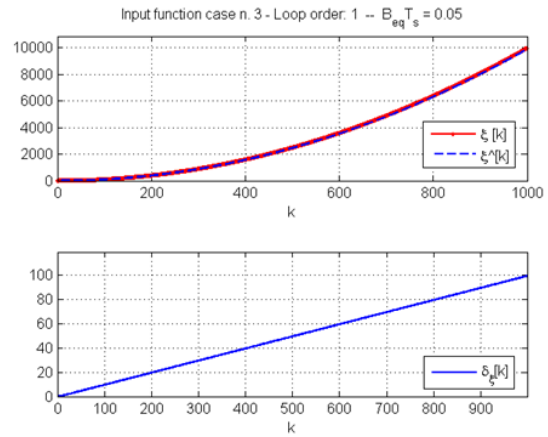


Figure 15. Plot of the steady state error  $\delta_\xi[k]$  for a parabolic input,  $B_{eq}T_s = 0.05$

### 3.4. Second order loop with a step input

The second order loop can correctly track both a step and a ramp input signal.

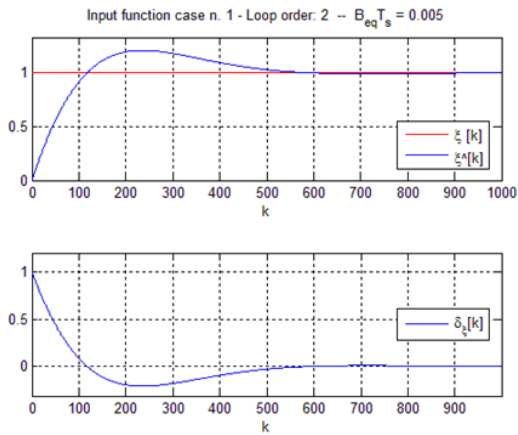


Figure 16. Second order loop with a step input,  $\zeta=0.707$

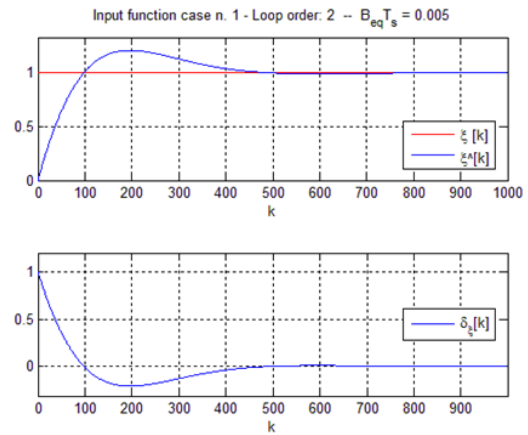


Figure 17. Second order loop with a step input,  $\zeta=1$

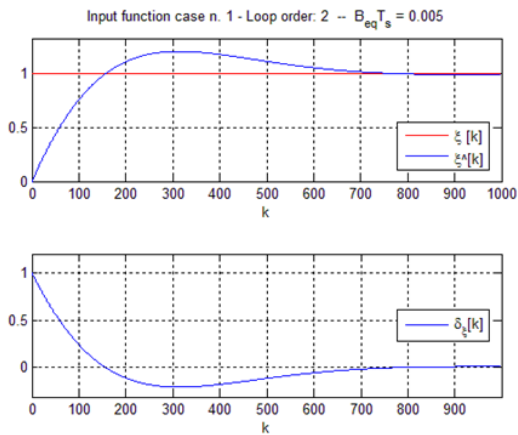


Figure 18. Second order loop with a step input,  $\zeta=0.5$

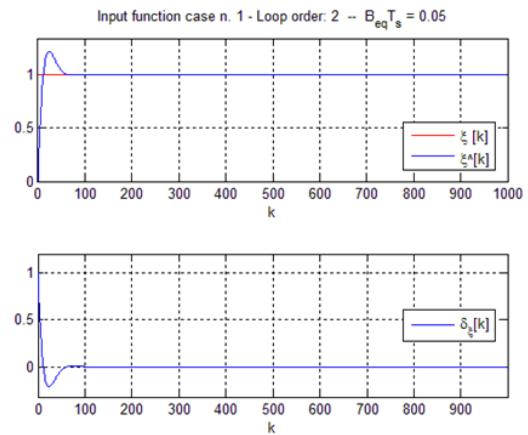


Figure 19. Second order loop with a step input,  $\zeta=0.707$ ,  $B_{eq}T_s=0.05$

In the simulation program were set  $B_{eq}T_s=0.005$ , second-order loop,  $\zeta=1/\sqrt{2}$ , then the program was run with a step input. The values of  $a$  and  $b$  as obtained by the program are:  $a = 0.0133$  and  $b = 0.0132$ . The values of  $\alpha$  and  $\alpha^*$  obtained by the program are:  $\alpha = 0.9933+i0.0066$  and  $\alpha^*=0.9933-i0.0066$ . Modulus and phase of the poles are:  $M=0.9934$  and  $\psi=0.0066$ . For  $k=99\div146$  we have that:  $-0.0977 < \delta_\xi[k] < 0.0958$ . From Figure 16, for  $k=117\div120$  we have that:  $-0.0060 < \delta_\xi[k] < 0.0069$ . For  $k=551\div999$  we have that:  $-0.01 < \delta_\xi[k] < 8.1952 \cdot 10^{-4}$ .

### 3.5. Second order loop with a ramp and quadratic input

Figure 20 depicts the estimation error for a ramp input and  $B_{eq}T_s=0.005$ . In Figure 21 is shown the estimation error plot for 1000 samples. It is observed a fast increase of the estimation error in the sampling interval (1-406) reaching its maximum value 234,9 for  $k = 406$ . After this interval the nearly steady-state is achieved for the remaining sampling interval. The value of steady-state error  $\delta_\xi[k]$  in this case observed in the deltaxi vector of values is 227.6 for the last sample  $k=999$ .

The only parameter that we can change in order to observe a difference in the reduction of the steady-state error is the second order loop filter's parameter  $\zeta$ . The differences of the steady-state values due to the changes of the  $\zeta$  parameter are shown in Table 4.

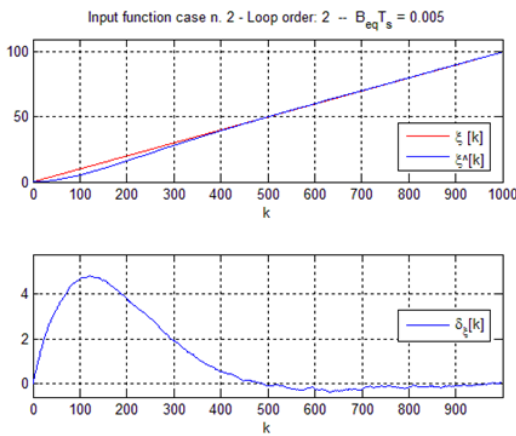


Figure 20. Plot of the estimation error for ramp input

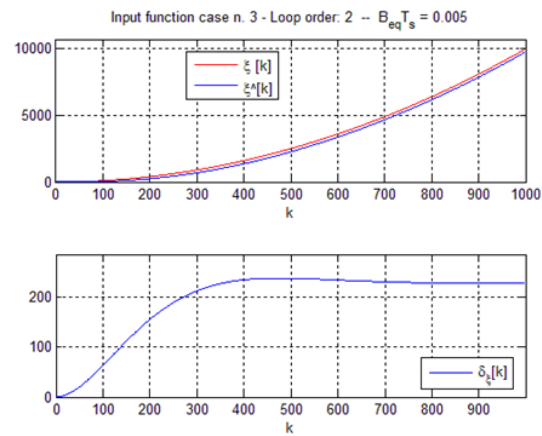


Figure 21. Plot of the estimation error for quadratic input

Table 4. The differences of the steady-state value due to the changes of the zeta parameter

Zeta value	$\delta_\xi[k]$
$\frac{1}{\sqrt{2}}$	227.63
$\frac{1}{2}$	405.99
2	115.03
4	105.19
8	102.81

Two main conclusions are derived from Table 4: First, with an increase of  $\zeta$  parameter, the steady-state error  $\delta_\xi[k]$  decreases in the same proportion, and second,  $\zeta$  equal to two is in a sort of way the value after which there is no significant decrease of the steady-state error.

Figure 22 shows that the simulation's estimation error follows nearly exactly the theoretical system response. Figure 23 shows the time evolution of the noise-free error which tends to reach zero if  $|1 - \beta\gamma| < 1$ .

## 4. Conclusion

In this article, the architecture of digital synchronizers for GPS receivers was studied. To evaluate the performance of the null-seeker, numerous simulation tests were performed. Three types of input signals were applied: step, ramp and parabolic. From the results we concluded that a higher noise equivalent bandwidth reduces the steady-state error, but this also reduces the integration time.

If it is expected that the parameter to be estimated is just an unknown constant, then a first-order loop is sufficient. If the parameter to be tracked varies linearly, then it is necessary to have at least a second-order loop.

If the parameter to be tracked has a quadratic variation, then it is necessary to have a third-order loop, but higher order loops may show instability problems. The conclusion is to choose the smallest order that guarantees a zero steady-state error in the considered application. For a second order loop, the steady state error for an input quadratic signal is constant. Considering the complexity in the design of high-order filters, our future work aims at studying the behavior of digital synchronizers for applications, in environments where the signal changes very quickly and in a non-deterministic way.

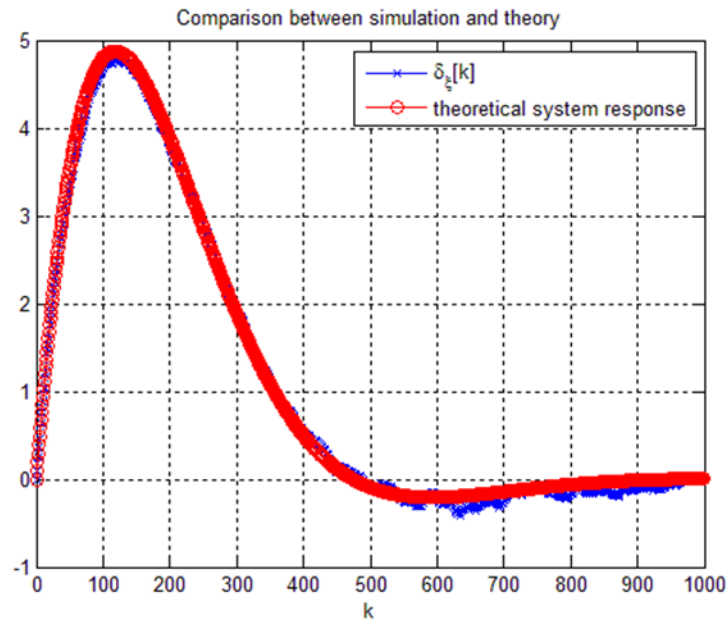


Figure 22. Comparison between simulation and theoretical system response

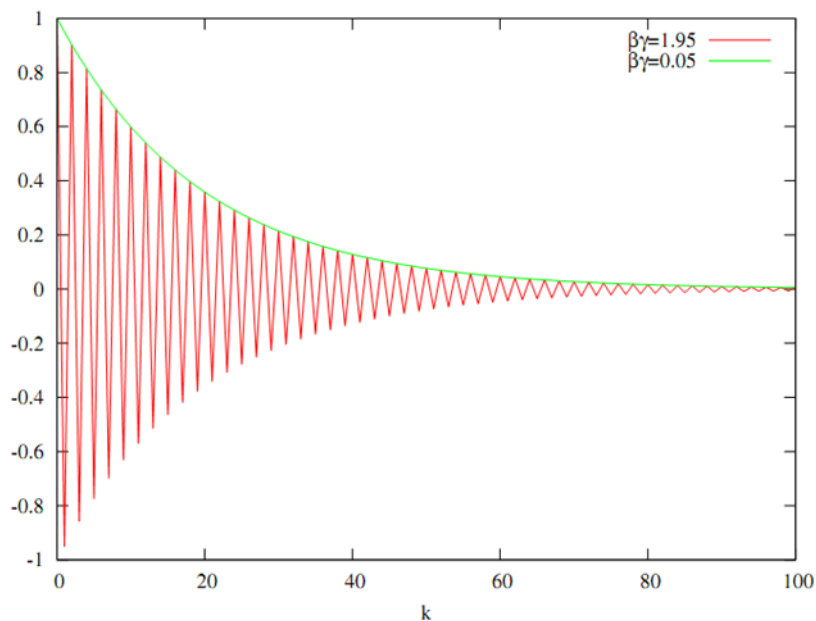


Figure 23. Time evolution of the noise-free error

### Acknowledgement

This study was partly presented at the 6<sup>th</sup> Advanced Engineering Days [10].

### Funding

This research received no external funding.

## Author contributions

**Alban Rakipi:** Conceptualization, Methodology, Software, Writing-Original draft preparation. **Olimpjon Shurdi:** Data curation, Software, Validation, Writing-Reviewing and Editing. **Aleksander Biberaj:** Visualization, Investigation, Writing-Reviewing and Editing.

## Conflicts of interest

The authors declare no conflicts of interest.

## References

1. Ögütçü, S., & Farhan, H. T. (2020). Assessing the contribution of galileo to gps+glonass single point positioning navigation. *El-Cezerî Journal of Science and Engineering*, 7(3), 1377-1383. <https://doi.org/10.31202/ecjse.754095>
2. Roncagliolo, P. A., Garcia, J. G., & Muravchik, C. H. (2012). Optimized Carrier Tracking Loop Design for Real-Time High-Dynamics GNSS Receivers. *International Journal of Navigation and Observation*, 651039. <https://doi.org/10.1155/2012/651039>
3. Won, J. H. & Pany, T. (2017). *Signal Processing*. Springer Handbooks.
4. Cheng, Y., & Chang, Q. (2020). A carrier tracking loop using adaptive strong tracking Kalman filter in GNSS receivers. *IEEE Communications Letters*, 24(12), 2903-2907. <https://doi.org/10.1109/LCOMM.2020.3018742>
5. Clare, A., Lin, T., & Lachapelle, G. (2017). Effect of GNSS receiver carrier phase tracking loops on earthquake monitoring performance. *Advances in Space Research*, 59(11), 2740-2749. <https://doi.org/10.1016/j.asr.2016.07.002>
6. Cheng, L., Dai, Y., Guo, W., & Zheng, J. (2021). Structure and performance analysis of signal acquisition and Doppler tracking in LEO augmented GNSS receiver. *Sensors*, 21(2), 525. <https://doi.org/10.3390/s21020525>
7. Curran, J. T. (2015). Enhancing Weak-Signal Carrier Phase Tracking in GNSS Receivers. *International Journal of Navigation & Observation*, 295029. <https://doi.org/10.1155/2015/295029>
8. Li, Z., Zhang, T., Qi, F., Tang, H., & Niu, X. (2019). Carrier phase prediction method for GNSS precise positioning in challenging environment. *Advances in space research*, 63(7), 2164-2174. <https://doi.org/10.1016/j.asr.2018.12.015>
9. Rakipi, A., Kamo, B., Cakaj, S., Lala, A., & Shinko, I. (2015, June). GPS signal acquisition and sensitivity analysis using different algorithms on a software receiver. In *2015 7th International Conference on Computational Intelligence, Communication Systems and Networks* (pp. 97-102). IEEE. <https://doi.org/10.1109/CICSyN.2015.27>
10. Rakipi, A., Shurdi, O., & Biberaj, A. (2023). Steady state error and equivalent noise bandwidth analysis of the null-seeker architecture for GPS receivers. *Advanced Engineering Days (AED)*, 6, 176-178.



© Author(s) 2023. This work is distributed under <https://creativecommons.org/licenses/by-sa/4.0/>